Enhancing the Area of a Raman Atom Interferometer Using a Versatile Double-Diffraction Technique

T. Lévèque, A. Gauguet,* F. Michaud, F. Pereira Dos Santos, and A. Landragin†

LNE-SYRTE, UMR 8630 CNRS, UPMC, Observatoire de Paris, 61 avenue de l'Observatoire, 75014 Paris, France

(Received 21 April 2009; published 21 August 2009)

In this Letter, we demonstrate a new scheme for Raman transitions which realize a symmetric momentum-space splitting of $4\hbar k$, deflecting the atomic wave packets into the same internal state. Combining the advantages of Raman and Bragg diffraction, we achieve a three pulse state labeled an interferometer, intrinsically insensitive to the main systematics and applicable to all kinds of atomic sources. This splitting scheme can be extended to $4N\hbar k$ momentum transfer by a multipulse sequence and is implemented on a $8\hbar k$ interferometer. We demonstrate the area enhancement by measuring inertial forces.

DOI: 10.1103/PhysRevLett.103.080405 PACS numbers: 03.75.Dg, 06.30.Gv, 37.25.+k, 67.85.−d

Atom interferometers are of interest for precision measurements of fundamental constants [1–4] and for inertial measurements [5,6]. The sensitivity of these apparatuses is closely related to the ability to diffract atomic wave packets in a coherent way. The angular splitting of this process determines the enclosed area of the interferometer and also its sensitivity. Many techniques have been implemented to coherently separate atomic waves and increase the angular deflection using material gratings [7], magneto-optical beam splitters [8,9], or momentum transfer by adiabatic passage [10]. For precision measurements, the use of two photon transitions is the most frequently used since they guarantee the control of the momentum transfer during the diffraction process.

Matter wave gratings made of a near resonant standing light wave permit the diffraction of the atoms along several coherent paths, separated by $2\hbar k$, in the Kapitza-Dirac or Bragg regime. As in this kind of interferometer [11–13] atoms always travel in the same internal state, the output phase shift is intrinsically insensitive to many systematics such as the ac Stark shift and temporal fluctuations of the Zeeman effect. These methods require the use of highly collimated atomic sources for detection on the external degree of freedom or careful analysis for a multiple path fringe pattern [13]. Alternatively, stimulated Raman transitions [14], which split a wave packet into two distinct internal states, are well adapted for use with noncollimated atomic sources such as optical molasses. In addition, they allow one to realize interferometers which benefit from an internal state labeling [15] for the output phase measurement, as populations of the output ports can be detected using a state selective technique.

Many improvements have been made to increase the momentum-space splitting of Bragg [12,16–20] and Raman [21] based interferometers. Recent works have also permitted an enhancement in the momentum-space splitting by using conventional Raman and Bragg schemes coupled to Bloch oscillations [22–25].

Here we demonstrate a new scheme based on Raman transitions, which achieves a symmetric momentum-space splitting of $4\hbar k$ (Fig. 1). It combines the advantages of these two methods. First, starting with atoms from an optical molasses, we realize an interferometer where partial wave packets propagate along its two arms in the same internal state. Second, the measurement of the output phase shift can still be realized thanks to the state labeling. The area of the interferometer is then increased by a factor of 2 compared to the traditional $\pi/2$-π-$\pi/2$ three pulse configuration. This scheme can be easily extended to perform a $4N\hbar k$ momentum splitting thanks to a multipulse sequence technique. As an example, we utilize a $8\hbar k$ interferometer for inertial measurements.

In our apparatus, described in Ref. [26], 10^7 cesium atoms are loaded from a vapor into two independent magneto-optical traps. Two cesium clouds are then launched at a temperature of 1.2 μK into two opposite parabolic trajectories using moving molasses at velocity $v = 2.4\ \mathrm{m \cdot s^{-1}}$, oriented at an angle of 8° with respect to the vertical direction. At the apex of their trajectory, the atoms interact with horizontal Raman laser pulses which

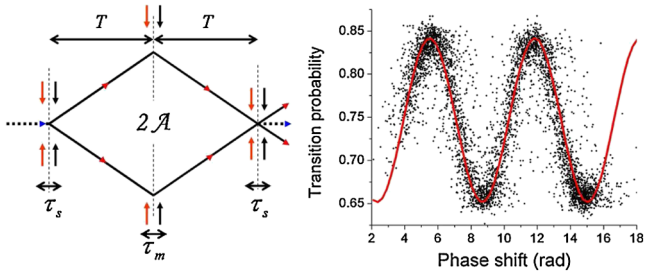

FIG. 1 (color online). Left: Scheme of the $4\hbar k$ interferometer realized using three double-diffraction pulses of duration τ_s, τ_m, and τ_s. Dotted and solid lines, respectively, represent wave packets in the state $|g\rangle$ and $|e\rangle$. Right: Interferometer signal for the source S_1 as a function of the phase shift calculated from the tilt meter signal.

act on the matter wave as beam splitters or mirrors and generate an interferometer with $2T = 60$ ms of total interaction time. The use of two atomic sources (S_1 and S_2) launched along opposite directions allows discrimination between the acceleration and rotation [6].

Raman transitions are implemented in a retroreflected geometry. The two laser beams of parallel polarizations at $\lambda = 852$ nm are guided to the setup through the same polarizing fiber. The beams pass through the vacuum chamber and are reflected by a mirror, crossing a quarter-wave plate twice. The wave plate is set in such a way that the reflected lasers have orthogonal linear polarization compared to the incident ones. As a result, counterpropagating Raman transitions are allowed while copropagating Raman transitions are forbidden. This commonly used geometry limits the impact of wave-front aberrations and provides a simple way to implement the k reversal technique [27]. In fact, in this scheme, atoms interact with four laser waves which drive Raman transitions with effective wave vectors $\pm\mathbf{k_{eff}} = \pm(\mathbf{k_1} - \mathbf{k_2})$.

Atoms are initially prepared in the ground state $|6S_{1/2}, F = 3, m_F = 0\rangle$, which is written as $|g\rangle$. Our four laser design efficiently couples this initial state to the excited state $|6S_{1/2}, F = 4, m_F = 0\rangle$ by transferring a $2\hbar k$ momentum along two opposite directions. The state $|g, p\rangle$ is then coupled to the two states $|e, p + 2\hbar k\rangle$ and $|e, p - 2\hbar k\rangle$, where p is the initial momentum state of the atom [26]. Because of the Doppler shift $\omega_D = (\mathbf{p} \cdot \mathbf{k}_{\mathrm{eff}})/M$, employing a retroreflected configuration allows the deflection of matter waves in only one momentum state or the other [5,26,28,29]. In our new method, we take advantage of a null Doppler shift to simultaneously couple the atoms in the two symmetric momentum states. This double-diffraction scheme results in a momentum splitting of $4\hbar k$ with the same internal state $|e\rangle$ in the two paths.

First, we investigate the efficiency of this beam splitter scheme by comparing experimental results and numerical simulations of the evolution of the atomic states, when interacting with the four laser waves. Figure 2 shows the measurement of the transition probability from the ground state $|g\rangle$ to the excited state $|e\rangle$ obtained for the atomic clouds as a function of pulse duration. The effective Rabi frequency, defined as usual [30], is $\Omega_{\mathrm{eff}} = 2.77 \times 10^4$ rad $\cdot$ s^{-1}. Experimental data are in good agreement with the results of a numerical calculation, displayed as a thick line, in which the basis states are restricted to five momentum states, adding the $|g, p \pm 4\hbar k\rangle$ detuned states to the three previous ones $|g\rangle$ and $|e, p \pm 2\hbar k\rangle$. We verified that the populations in the higher momentum states are negligible taking into account our experimental parameters. We consider the case in which the frequency difference between the lasers is set to $\delta\omega_1 = (\omega_e - \omega_g) + \omega_R$, where $\omega_R = (\hbar k_{\mathrm{eff}}^2)/2M$ is the recoil frequency. By extension of the calculation presented in Ref. [30], we solve the Schrödinger equation and calculate the evolution of the populations. The calculation takes into account the Doppler shift linked to the velocity dispersion of the atoms and the spatial dependence of Ω_{eff} due to the expansion of the atomic clouds in the Gaussian profile of the Raman beam. In order to keep only the atoms in the two symmetric states $|e, p \pm 2\hbar k\rangle$, a pushing beam is implemented after the Raman pulse so as to remove remaining atoms in the ground state $|g\rangle$. In addition, using this scheme, we have verified on the experiment that the beam splitter also realizes a velocity selection of the input momentum state (5.9 mm $\cdot$ s^{-1} FWHM).

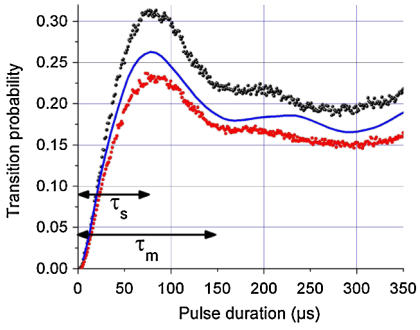

FIG. 2 (color online). Rabi oscillation profiles obtained for the two atomic sources S_1 and S_2 at the apex of their trajectory (dots). The curve is the result of a numerical simulation.

Using this double-diffraction scheme, we realize an interferometer with a three pulse sequence (Fig. 1). The first pulse of duration $\tau_s = \pi/\sqrt{2}\Omega_{\mathrm{eff}}$ splits the input state $|g, p\rangle$ into $|e, p \pm 2\hbar k\rangle$ symmetrically. The second pulse of duration $\tau_m = \sqrt{2}\pi/\Omega_{\mathrm{eff}}$ acts as a mirror by coupling each path to its opposite momentum state. Finally, matter waves are recombined thanks to a third pulse, of duration τ_s, to form a symmetric interferometer in which the matter waves propagate in the same internal state $|e\rangle$. A pushing beam is implemented after each of the two first Raman pulses so as to suppress spurious interferometers. An important feature of this Raman transition scheme is the use of state labeling at the output of the interferometer even if the matter waves travel in the same internal state. The output phase shift can thus easily be measured thanks to a fluorescence technique. The output atomic phase shift of our device is sensitive to acceleration a and rotation Ω as $\Delta\Phi = 2\mathbf{k_{eff}} \cdot [\mathbf{a} - 2(\mathbf{v} \times \mathbf{\Omega})]T^2$ [26], increasing the sensitivity of the traditional $\pi/2$-π-$\pi/2$ three pulse geometry by a factor of 2.

Similar to a Bragg interferometer, our apparatus is, in principle, insensitive to the main systematic effects: ac Stark shift, temporal fluctuations of the Zeeman effect, and a magnetic field gradient along the direction of propagation of the atomic cloud. Moreover, the interferometer phase does not depend on the laser phase difference as its influence is identical over the two paths.

In order to scan the phase, a controlled acceleration phase shift is induced on the interferometer. This is simply

achieved by tilting the apparatus (± 50 μrad) to get a small projection of the gravity along the axis of the light pulses. The inclination is measured thanks to a calibrated tilt meter (Applied Geomechanics 701-2A). In Fig. 1 is displayed the transition probability as a function of the phase shift deduced from the tilt measurement. We observed a contrast of 20% identical for the two atomic sources, attributed to inhomogeneity of the Raman intensity over the atomic cloud.

Using horizontal Raman beams makes the interferometer sensitive to the vertical component of the Earth rotation rate $\Omega_z^E = 5.49 \times 10^{-5}$ rad $\cdot$ s^{-1} at the latitude of Observatoire de Paris. The quadratic scaling of the rotation and acceleration phase shifts with the interaction time T is verified from $T = 10$ to 30 ms (Fig. 3). The fits of experimental phase shifts give measurements of the scale factors compatible with the expected values, respectively, to 3% and 4% for acceleration and rotation. We deduce a rotation rate of $\Omega_z = 5.75 \times 10^{-5}$ rad $\cdot$ s^{-1} in agreement with the expected projection of Earth's rotation rate within the error bar.

The double-diffraction scheme can be extended to higher momentum-space splitting thanks to the retroreflected configuration. After splitting the atoms into the two symmetric states $|e, p \pm 2\hbar k\rangle$ with the first pulse, a second pulse can be implemented to efficiently couple these two resulting states to the next momentum states $|g, p \pm 4\hbar k\rangle$. The Raman frequency difference of the second pulse has to be changed to $\delta\omega_2 = (\omega_e - \omega_g) - 3\omega_R$ in order to fulfill the resonance condition between the momentum states and the two pairs of Raman lasers. This scheme can be extended to a N pulse sequence to reach up to $4N\hbar k$ momentum-space splitting. In order to conserve the resonance condition, the Raman frequency difference of the ith pulse has to be changed and set to $\delta\omega_i = (\omega_e - \omega_g) + (-1)^{i-1}(2i - 1)\omega_R$. Following this argument, symmetric Raman transitions are suitable to realize a large area interferometer with $4N\hbar k$ momentum-space splitting.

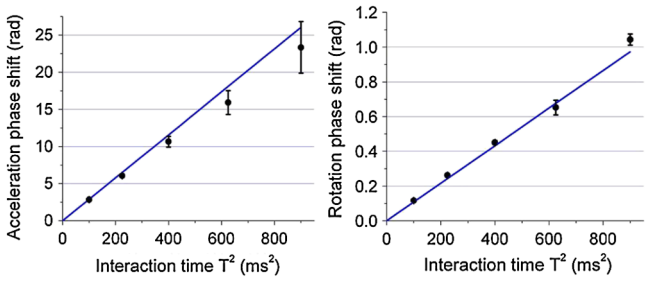

FIG. 3 (color online). Quadratic scaling of the acceleration phase shift induced by the projection of g for an angle of 100 μrad with respect to the horizontal plane (left) and of the rotation phase shift induces by the vertical component of the rotation rate Ω_z^E (right) as a function of the interaction time T^2. The measurements (dots) are compared with the expected behaviors (lines).

Here we demonstrate an interferometer realized with $N = 2$, reaching a $8\hbar k$ momentum-space splitting between the two paths, using seven Raman pulses. In this configuration (Fig. 4), the first atomic beam splitter is composed of two light pulses, respectively, set with detunings $\delta\omega_1$ and $\delta\omega_2$. In this manner, matter waves are coupled from the state $|g, p\rangle$ to $|g, p \pm 4\hbar k\rangle$. The mirror is realized by three successive pulses at $\delta\omega_2$, $\delta\omega_1$, and $\delta\omega_2$ in order to deflect the atoms in their opposite momentum state. Finally, the two interferometric paths are recombined with the symmetric $\delta\omega_2$, $\delta\omega_1$ light-pulse sequence. The durations of the seven pulses are, respectively, τ_s, τ_π, τ_π, τ_m, τ_π, τ_π, and τ_s, where $\tau_\pi = \pi/\Omega_{\text{eff}}$. In addition, four pushing pulses are applied to blow away residual atoms remaining in the internal state $|g\rangle$.

The total interaction time of this interferometer is $2T = 60$ ms. Atoms propagate in the states $|g, p \pm 4\hbar k\rangle$ during $2\delta t = 40$ ms with a delay of $(T - \delta t)/2$. The interferometric area increases by a factor of $\alpha = 2(1 + \delta t/T)$ compared with the $\pi/2$-π-$\pi/2$ configuration. The sensitivity to inertial effects is then proportionally enhanced up to $\Delta\Phi = \alpha \mathbf{k_{eff}} \cdot [\mathbf{a} - 2(\mathbf{v} \times \mathbf{\Omega})]T^2$. As before, this phase is scanned by tilting the interferometer. In Fig. 5, we show the fringe patterns of the two sources, obtained with the $8\hbar k$ interferometer. The phase shift between the two interferometers corresponds to the rotation phase shift induced by the vertical component of the Earth rotation rate Ω_z^E. The linear scaling of the acceleration phase shift with α was investigated by changing δt. Figure 5 displays the result of the measurement for $\delta t = 0$–20 ms which shows good agreement with the expected slope within 2%. This corresponds to an enhanced sensitivity of a factor of 3.46 compared to the usual $\pi/2$-π-$\pi/2$ configuration.

With respect to the $4\hbar k$ case of a three pulse interferometer, the atoms do not remain into the same internal state all along the two paths. Nevertheless, as the internal state changes at the same time for the two partial wave packets,

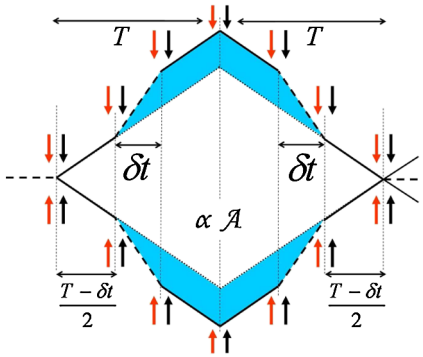

FIG. 4 (color online). Recoil diagram for the $8\hbar k$ interferometer reaching a total area enhanced by a factor of α. Dotted lines represent wave packets in the $|g\rangle$ hyperfine ground state, while solid lines depict the $|e\rangle$ ground state. The colored surface represents the area enhancement compared with the corresponding three pulse configuration.

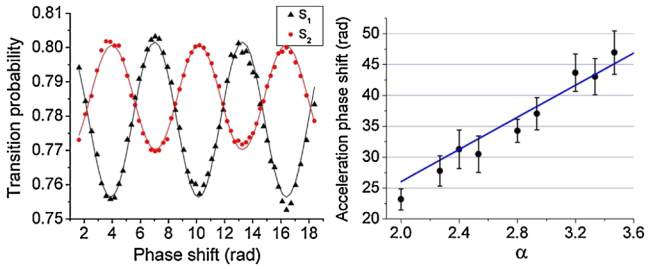

FIG. 5 (color online). Left: Fringe patterns averaged over 450 samples. Right: Linear scaling of the acceleration phase shift induced by the projection of g for an angle of 100 μrad with respect to the horizontal plane as a function of the area enhancement factor α. The measurement (dots) is compared with the expected values (line).

the enhanced interferometer remains insensitive to the same systematics as in the Bragg case.

In conclusion, we demonstrated a new method of achieving symmetric Raman transitions with $4\hbar k$ momentum-space splitting, deflecting the atoms into the same internal state. Using this double-diffraction technique, we have realized an interferometer of increased area which has been tested by performing acceleration and rotation measurements. The splitting scheme has been extended to reach a $8\hbar k$ interferometric geometry in a seven pulse configuration, opening the way for enhanced $4N\hbar k$ path separation geometry.

This scheme provides a simple way to increase the sensitivity of the apparatus without any significant changes in the experimental setup thanks to the retroreflected Raman configuration. In particular, it does not require extra laser power compared to standard Raman transition based interferometers, in contrast with other methods. Furthermore, as matter waves are symmetrically driven in the same ground state, interferometers are intrinsically insensitive to the ac Stark shift, the Zeeman effect, and Raman laser phase noise. The enhanced area geometry thus combines the advantages of Raman and Bragg based interferometers. Moreover, the principle of double diffraction can be extended to the case of a nonzero Doppler shift, providing that the two opposite Raman transitions remain resonant simultaneously. This general case requires at least three different laser frequencies.

Finally, this work provides insight into space-atom interferometer design [28]. Indeed, for inertial sensors in zero-gravity environments, the Doppler effect cannot be used to select one or the other effective Raman transitions in the current retroreflected configuration needed for accuracy [29]. The symmetric Raman diffraction offers a promising solution to circumvent this constraint.

We thank the Institut Francilien pour la Recherche sur les Atomes Froids (IFRAF) and the European Union (FINAQS STREP/NEST project Contract No. 012986 and EuroQUASAR/IQS project) for financial support. T. L. thanks the DGA for supporting his work. We also thank P. Bouyer for careful reading.

*Present address: Department of Physics, Durham University, Rochester Building, South Road, Durham DH1 3LE, United Kingdom.
†arnaud.landragin@obspm.fr

[1] A. Wicht *et al.*, Phys. Scr. **T102**, 82 (2002).
[2] P. Cladé *et al.*, Phys. Rev. Lett. **96**, 033001 (2006).
[3] J. B. Fixler *et al.*, Science **315**, 74 (2007).
[4] G. Lamporesi *et al.*, Phys. Rev. Lett. **100**, 050801 (2008).
[5] A. Peters, K. Y. Chung, and S. Chu, Metrologia **38**, 25 (2001).
[6] T. L. Gustavson, A. Landragin, and M. A. Kasevich, Classical Quantum Gravity **17**, 2385 (2000).
[7] D. W. Keith *et al.*, Phys. Rev. Lett. **66**, 2693 (1991).
[8] T. Pfau *et al.*, Phys. Rev. Lett. **71**, 3427 (1993).
[9] T. Schumm *et al.*, Nature Phys. **1**, 57 (2005).
[10] M. Weitz, B. C. Young, and S. Chu, Phys. Rev. Lett. **73**, 2563 (1994).
[11] E. M. Rasel *et al.*, Phys. Rev. Lett. **75**, 2633 (1995).
[12] D. M. Giltner, R. W. McGowan, and S. A. Lee, Phys. Rev. Lett. **75**, 2638 (1995).
[13] S. B. Cahn *et al.*, Phys. Rev. Lett. **79**, 784 (1997).
[14] M. Kasevich, and S. Chu, Phys. Rev. Lett. **67**, 181 (1991).
[15] Ch. J. Bordé, Phys. Lett. A **140**, 10 (1989).
[16] A. Miffre *et al.*, Eur. Phys. J. D **33**, 99 (2005).
[17] A. E. A. Koolen *et al.*, Phys. Rev. A **65**, 041601(R) (2002).
[18] Y. J. Wang *et al.*, Phys. Rev. Lett. **94**, 090405 (2005).
[19] S. Gupta *et al.*, Phys. Rev. Lett. **89**, 140401 (2002).
[20] H. Müller *et al.*, Phys. Rev. Lett. **100**, 180405 (2008).
[21] J. M. McGuirk, M. J. Snadden, and M. A. Kasevich, Phys. Rev. Lett. **85**, 4498 (2000).
[22] P. Cladé *et al.*, Phys. Rev. Lett. **102**, 240402 (2009).
[23] H. Müller *et al.*, Phys. Rev. Lett. **102**, 240403 (2009).
[24] B. Dubetsky and P. R. Berman, Phys. Rev. A **66**, 045402 (2002).
[25] T. Salger *et al.*, Phys. Rev. A **79**, 011605(R) (2009).
[26] B. Canuel *et al.*, Phys. Rev. Lett. **97**, 010402 (2006).
[27] D. S. Durfee, Y. K. Shaham, and M. A. Kasevich, Phys. Rev. Lett. **97**, 240801 (2006).
[28] See, for instance, Special issue on Quantum Mechanics for Space Application: From Quantum Optics to Atom Optics and General Relativity, edited by P. Bouyer and A. Bresson [Appl. Phys. B **84** 2006].
[29] A. Landragin and F. Pereira Dos Santos, in *Atom Optics and Space Physics*, Proceedings of the International School of Physics "Enrico Fermi," Course CLXVIII, edited by E. Arimondo, W. Ertmer, E. M. Rasel, and W. P. Schleich (IOS Press, Amsterdam, 2009).
[30] K. Moler *et al.*, Phys. Rev. A **45**, 342 (1992).